Monthly Notices
of the
ROYAL ASTRONOMICAL SOCIETY

MNRAS **474,** 2109–2115 (2018)
Advance Access publication 2017 October 24

doi:10.1093/mnras/stx2723

Constraining the baryon–dark matter relative velocity with the large-scale three-point correlation function of the SDSS BOSS DR12 CMASS galaxies

Zachary Slepian,[1]★ Daniel J. Eisenstein,[1]★ Jonathan A. Blazek,[2] Joel R. Brownstein,[3] Chia-Hsun Chuang,[4,5] Héctor Gil-Marín,[6,7] Shirley Ho,[8,9,10] Francisco- Shu Kitaura,[5] Joseph E. McEwen,[2] Will J. Percival,[11] Ashley J. Ross,[2] Graziano Rossi,[12] Hee-Jong Seo,[13] Anže Slosar[14] and Mariana Vargas-Magaña[15]

[1]*Harvard–Smithsonian Center for Astrophysics, 60 Garden Street, Cambridge, MA 02138, USA*
[2]*Center for Cosmology and Astroparticle Physics, Department of Physics, The Ohio State University, OH 43210, USA*
[3]*Department of Physics and Astronomy, University of Utah, Salt Lake City, UT 84112, USA*
[4]*Instituto de Física Teórica, (UAM/CSIC), Universidad Autónoma de Madrid, Cantoblanco, E-28049 Madrid, Spain*
[5]*Leibniz-Institut für Astrophysik Potsdam (AIP), An der Sternwarte 16, D-14482 Potsdam, Germany*
[6]*Sorbonne Universités, Institut Lagrange de Paris (ILP), 98 bis Boulevard Arago, F-75014 Paris, France*
[7]*Laboratoire de Physique Nucléaire et de Hautes Energies, Université Pierre et Marie Curie, 4 Place Jussieu, F-75005 Paris, France*
[8]*Lawrence Berkeley National Lab, 1 Cyclotron Road, Berkeley, CA 94720, USA*
[9]*McWilliams Center for Cosmology, Department of Physics, Carnegie Mellon University, 5000 Forbes Ave., Pittsburgh, PA 15213, USA*
[10]*Department of Physics, University of California, Berkeley, CA 94720, USA*
[11]*Institute of Cosmology and Gravitation, University of Portsmouth, Dennis Sciama Building, Portsmouth PO1 3FX, UK*
[12]*Department of Physics and Astronomy, Sejong University, Seoul 143-747, Korea*
[13]*Department of Physics and Astronomy, Ohio University, Clippinger Labs, Athens, OH 45701, USA*
[14]*Brookhaven National Laboratory, Upton, NY 11973, USA*
[15]*Instituto de Física, Universidad Nacional Autónoma de México, Apdo. Postal 20-364, Mexico 04510, Mexico*

Accepted 2017 October 12. Received 2017 September 15; in original form 2017 February 13

ABSTRACT

We search for a galaxy clustering bias due to a modulation of galaxy number with the baryon–dark matter relative velocity resulting from recombination-era physics. We find no detected signal and place the constraint $b_v < 0.01$ on the relative velocity bias for the CMASS galaxies. This bias is an important potential systematic of baryon acoustic oscillation (BAO) method measurements of the cosmic distance scale using the two-point clustering. Our limit on the relative velocity bias indicates a systematic shift of no more than 0.3 per cent rms in the distance scale inferred from the BAO feature in the BOSS two-point clustering, well below the 1 per cent statistical error of this measurement. This constraint is the most stringent currently available and has important implications for the ability of upcoming large-scale structure surveys such as the Dark Energy Spectroscopic Instrument (DESI) to self-protect against the relative velocity as a possible systematic.

Key words: cosmological parameters – cosmology: observations.

1 INTRODUCTION

Prior to decoupling at redshift $z \sim 1020$, baryons and dark matter behave differently because they experience different forces. The Universe is ionized, and the electrons are tightly coupled to the photons through Thomson scattering, while the protons follow the electrons under the Coulomb force. On scales within the sound horizon, the baryons are supported against gravitational infall by the photon pressure, which is large because the photons are an important component of the energy density and are relativistic.

Consider the evolution of a point-like density perturbation in an otherwise homogeneous Universe. It will create a photon overpressure that launches a pulse of baryons and photons outwards (i.e. produce a baryon acoustic oscillation, BAO), and this pulse's front will be at the sound horizon (Sakharov 1966; Peebles & Yu 1970; Sunyaev & Zel'dovich 1970; Bond & Efstathiou 1984, 1987; Holtzmann 1989; Hu & Sugiyama 1996; Eisenstein & Hu 1998; Eisenstein, Seo & White 2007; Slepian & Eisenstein 2016).

Baryons and photons farther away from the overdensity than the sound horizon will not yet know about the overpressure, and so they

★ E-mail: zslepian@lbl.gov (ZS); deisenstein@cfa.harvard.edu (DE)

must infall under gravity. Meanwhile, the dark matter is insensitive to the photon pressure and infalls under gravity on all scales. As a result, when the photons release the baryons at decoupling, the dark matter within the sound horizon has a head start on infalling towards the initial density perturbation: There is a baryon–dark matter relative velocity on scales within the sound horizon.

The magnitude of this relative velocity depends on the magnitude of the initial density perturbation. Therefore, different regions of the Universe have different relative velocities, and these velocities are coherent on sound-horizon ($100\,\mathrm{Mpc}\,h^{-1}$) scales. The relative velocity effect was first calculated by Tseliakhovich & Hirata (2010), and shortly after (Dalal, Pen & Seljak 2010; Yoo, Dalal & Seljak 2011), it was shown that this relative velocity can shift the BAO signal in the two-point clustering if the late-time luminous red galaxies (LRGs) used for these measurements have strong memories of their earliest progenitors.

In particular, the relative velocity's root mean square value at $z \sim 50$, when the first galaxies are expected to form, is of the order of 10 per cent of the smallest $10^6\,\mathrm{M}_\odot$ dark matter haloes' circular velocities or velocity dispersions. Thus, small dark matter haloes living in a region of high relative velocity will find it difficult to capture baryons: the baryons' kinetic energy in the dark matter's rest frame is too large. The relative velocity can therefore induce an additional modulation of the clustering of these primordial galaxies on scales out to the BAO scale of $100\,\mathrm{Mpc}\,h^{-1}$. This modulation adds or subtracts from the primordial two-point correlation function (2PCF) within the BAO scale but not outside, and so can shift the BAO bump in or out in physical scale (this configuration space picture was developed in Slepian & Eisenstein 2015a, hereafter SE15a). If the late-time LRGs used for the BAO method at present have a strong memory of their early, small progenitors, the relative velocity can therefore bias the measured cosmic distance scale.

Note that the relative velocity is fundamentally an effect set by the relativistic sound speed prior to decoupling; thus, its large-scale coherence is unique and cannot be substantially modified by later-time feedback processes or non-linear structure formation as they operate on far smaller scales. Recent work on this bias has shown that even a small coupling of the relative velocity to late-time galaxy formation can induce a substantial shift in the distance scale (Blazek, McEwen & Hirata 2016, hereafter BMH16). Further work (Schmidt 2016, hereafter S16) pointed out that even at linear order the divergence of the relative velocity $\theta_{\rm bc}$ as well as the isocurvature mode $\delta_{\rm b} - \delta_{\rm c}$ also enters the bias model, although this latter term is not expected to significantly shift the BAO position. The velocity divergence term of S16 is effectively present in BMH16 but with a fixed rather than free amplitude given by a loop integral. S16 found that this coefficient may be even larger than that computed by BMH16; thus the BMH16 BAO scale shifts in the power spectrum likely represent a lower bound on the relative velocity's true impact on the BAO scale as measured from two-point clustering.

Yoo et al. (2011) proposed that the bispectrum (Fourier space analogue of the 3PCF) could be used to measure the relative velocity bias and then correct any effect in the 2PCF, but up to now this technique has not been used. Yoo & Seljak (2013) used the power spectrum of galaxies to constrain the relative velocity bias in their bias model to be less than 0.033; due to different normalization conventions, this translates into a b_v constraint in our bias model of 0.1, as we further detail in Section 5. Beutler et al. (2016) compared overlapping redshift slices within the Baryon Oscillation Spectroscopic Survey (BOSS) and WiggleZ to look for the relative velocity effect and found no evidence for it. Around the same time as our study here, Beutler, Seljak & Vlah (2017) searched for a possible shift in the CMASS power spectrum, including the $\theta_{\rm bc}$ and $\delta_{\rm bc}$ terms in the bias model. They found no evidence for these terms and constrained any possible shift induced by the RV to similar precision as this work.

To give a quantitative sense of the possible impact of a relative velocity bias, we note that BMH16 show that even a relative velocity bias of the order of 4 per cent of the linear bias can cause a 1 per cent shift in the distance scale, comparable with the statistical errors on the latest BOSS measurement (Alam et al. 2017; Cuesta et al. 2016; Gil-Marín et al. 2016). Further, the Dark Energy Spectroscopic Instrument (DESI; Levi et al. 2013), with first light in 2019, will improve on the BOSS error bars by roughly a factor of 5, so even a relative velocity bias that is 1 per cent of the linear bias could systematically shift the distance scale comparably to DESI's statistical error bars. Given that any robustly detected deviation of the dark energy equation of state w from -1 would have profound consequences for our understanding of dark energy, a high precision on the relative velocity bias is required.

In this work, we use the 3PCF technique first proposed in Yoo et al. (2011) and developed further in SE15a to constrain the relative velocity bias to be ≤ 0.01 for the SDSS BOSS DR12 CMASS galaxies (Eisenstein et al. 2011, for SDSS-III overview; Alam et al. 2015 for DR11 and DR12). This precision is sufficient to ensure that the cosmic distance scale measurement from BOSS will not be systematically biased. It also suggests that our technique is powerful enough to allow DESI to avoid this bias. Our measurement is the most stringent constraint on the relative velocity bias available, and illustrates the power of the 3PCF for relative velocity constraints. To make these measurements we used the $\mathcal{O}(N^2)$ 3PCF algorithm of Slepian & Eisenstein (2015b), with N the number of points. This algorithm is further developed in Slepian & Eisenstein (2015c) to exploit the speed of Fourier Transforms (FTs); however in the present work we use the $\mathcal{O}(N^2)$, non-FT version.

This paper is laid out as follows. Section 2 briefly outlines the galaxy sample and triangle configurations used for our analysis. In Section 3, we present our galaxy bias model including relative velocity bias. Section 4 describes our relative velocity constraint, discusses the other bias parameters and reports the cosmic distance scale measured with this bias model. We conclude in Section 5.

2 GALAXY SAMPLE AND TRIANGLE CONFIGURATIONS USED

We now briefly outline the galaxy sample used for this analysis as well as the specific triangle configurations used for our parameter constraints. Both topics are covered in greater depth in our companion paper Slepian et al. (2017b); see also Slepian et al. 2017a for our 3PCF measurement for the same sample in a compressed basis. Here we simply recapitulate the key points for completeness. The galaxy sample was the CMASS sample (Alam et al. 2015) within SDSS BOSS DR12 (Eisenstein et al. 2011; Dawson et al. 2013) made up of 777 202 LRGs over 9.493 deg^2 (Reid et al. 2016), which were colour-selected to have an approximately constant stellar mass $M_* > 10^{11}\,\mathrm{M}_\odot$. The sample spans the redshift range 0.43–0.7 and is roughly symmetric about 057. Target selection, catalogue construction and the random catalogues used to quantify the survey geometry are described in more detail in Reid et al. (2016). Ross et al. (2017) analyse observational systematics and the random catalogues.

The SDSS (York et al. 2000) comprised three parts: SDSS I and II (Abazajian et al. 2009) and SDSS III (Eisenstein et al. 2011). The survey imaged 14 555 deg^2 in five photometric bandpasses (Fukugita et al. 1996; Smith et al. 2002; Doi et al. 2010) with a

drift-scanning mosaic CCD camera (Gunn et al. 1998) on the 2.5-m Sloan Telescope (Gunn et al. 2006) at the Apache Point Observatory in New Mexico. Details of the astrometric calibration are given in Pier et al. (2003), the photometric reduction in Lupton et al. (2001) and the photometric calibration in Padmanabhan et al. (2008). The entire data set was reprocessed for DR8 as described in Aihara et al. (2011). Target assignment for BOSS was done via an adaptive algorithm presented in Blanton et al. (2003) and spectroscopy via double-armed spectrographs (Smee et al. 2013), with redshifts derived as described in Bolton et al. (2012).

An additional important component of our analysis was verification of both the pipeline and the covariance matrix using mock catalogues; these also offered an additional avenue to derive an error bar on our relative velocity constraint, as we discuss further in Section 4. These mocks, known as the MULTIDARK-PATCHY BOSS DR12 mocks (Kitaura, Yepes & Prada 2014; Kitaura et al. 2015), were developed for DR12, and use second-order Lagrangian perturbation theory (2LPT) combined with a spherical collapse model on small scales (Kitaura & Heß 2013) and additional calibration on *N*-body-based-reference catalogues. This calibration enabled the mocks to reproduce the number density, clustering bias, selection function and survey geometry of the BOSS data (Rodríguez-Torres et al. 2016).

We chose a subset of triangle side-length combinations to ensure that the scales used in the analysis are under good perturbative control, and hence that our parameter constraints will not be biased by breakdowns of the model. We restricted the smallest triangle side to be larger than 20 Mpc h^{-1} and the largest to be 140 Mpc h^{-1}. The former criterion is to avoid squeezed triangles where two galaxies are close enough together that their clustering is unlikely to be well-described by perturbation theory, and the latter cut is driven by the concern that our covariance matrix may begin to break down on larger scales, likely due to boundary effects, as well as the fact that the signal-to-noise ratio at these scales is sharply falling.

We thus use the set $\boldsymbol{S}$ of twenty bin combinations satisfying the above criteria: $\boldsymbol{S} = \{[2, 5], [2, 6], [2, 7], [2, 8], [2, 9], [2, 10], [2, 11], [2, 12], [3, 6], [3, 7], [3, 8], [3, 9], [3, 10], [3, 11], [4, 7], [4, 8], [4, 9], [4, 10], [5, 8], [5, 9]\}$. Bin 0 in r_1 would mean $0 \leq r_1 < 10\,\mathrm{Mpc}\,h^{-1}$, bin 1 in r_1 would mean $10 \leq r_1 < 20\,\mathrm{Mpc}\,h^{-1}$, etc., and analogously for r_2.

In this analysis, we do not use the galaxy 2PCF or power spectrum. We fix σ_8 to its value from Planck, rescaled to the average survey redshift of 0.57, and we fix f, the logarithmic derivative of the linear growth rate, to the value implied by Ω_m at the survey redshift. At fixed f, the redshift space distortions parameter $\beta = f/b_1$ depends on the linear bias, which is not known a priori. Our fitting procedure was therefore to fix β, derive b_1 and iterate until self-consistent β and b_1 were reached. The transfer functions were computed from CAMB (Code for Anisotropies in the Cosmic Microwave Background; Lewis 2000) using a geometrically flat ΛCDM cosmology with parameters matching those used for the MULTIDARK-PATCHY mock catalogues (Kitaura et al. 2015, 2016) and consistent with the Planck values. Our cosmology also matches that used for S15. The parameters are $\Omega_\mathrm{b} = 0.048, \Omega_\mathrm{m} = 0.307\,115$, $h \equiv H_0/(100\,\mathrm{km\,s^{-1}\,Mpc^{-1}}) = 0.6777, n_\mathrm{s} = 0.9611, \sigma_8(z = 0) = 0.8288, T_\mathrm{CMB} = 2.7255\,\mathrm{K}$.

3 RELATIVE VELOCITY BIAS MODEL

Following SE15a and Slepian & Eisenstein (2017; hereafter SE17), the galaxy overdensity field δ_g traces the matter density field δ_m and its square with two unknown bias coefficients, the linear bias b_1 and the non-linear bias b_2. The galaxy overdensity also traces the square of the local relative velocity with a third unknown bias coefficient, the relative velocity bias b_v. Note that at leading order in perturbation theory, the predicted 3PCF is the same whether one uses the Lagrangian or Eulerian relative velocity, as further discussed in SE17 Section 5. The bias model is

$$\delta_\mathrm{g}(\boldsymbol{x}) = b_1\delta_\mathrm{m}(\boldsymbol{x}) + b_2\left[\delta^2_\mathrm{m}(\boldsymbol{x}) - \left\langle\delta^2_\mathrm{m}(\boldsymbol{x})\right\rangle\right] + b_v\left[v^2_\mathrm{s}(\boldsymbol{x}) - 1\right], \quad (1)$$

where $v^2_\mathrm{s}(\boldsymbol{x}) \equiv v^2_\mathrm{bc}(\boldsymbol{x})/\sigma^2_\mathrm{bc}$ is the relative velocity's square v^2_bc normalized by its mean square value σ^2_bc. δ_m is the matter density field, which itself must be expanded to second-order in the linear density field δ as further discussed in SE15a and SE17. This bias model does not include tidal tensor biasing, for which our companion paper (Slepian et al. 2017, hereafter S17b) found mild evidence. Future work may be incorporating a tidal tensor bias into the RV constraint; for now we note that the tidal tensor itself contributes broad-band features to the 3PCF, whereas the RV has a sharp, distinctive signature. We therefore do not expect adding a tidal tensor bias to substantially change the RV constraint. As a comparison of figs 7 and 10 of SE17 shows, the tidal tensor bias has a very different triangle side length and multipole dependence from the relative velocity bias; tidal tensor is very broad-band, whereas the relative velocity has sharp features in scale. Furthermore, the tidal tensor constraint found in the companion paper S17b is driven by the $\ell = 2$ multipole of the 3PCF, whereas the relative velocity constraint presented here is driven by the $\ell = 1$ multipole. These points lead us to believe that there is very little degeneracy between the two biases, and we thus expect that incorporating tidal tensor bias would not alter the constraints found here.

Using the bias model (1), one can compute the 3PCF model including the relative velocity to lowest (fourth) order in the linear density field and including large-scale redshift-space distortions. Details of this computation and the resulting model are in SE17.

We note that our 3PCF model requires as an input $\beta = f/b_1 \approx \Omega_\mathrm{m}^{0.55}$, with $f = \mathrm{d\ln}D/\mathrm{d\ln}a$, a the scalefactor and D the linear growth rate. For reasons discussed in S17b Section 6.2, we elect to fix β at the beginning of our fitting, meaning that after obtaining b_1 from the fitting we must check that β is self-consistent. Here, we adopt two different β values: for the data, $\beta = 0.44$, whereas for the mocks, $\beta = 0.40$, which is consistent with the fitted value of b_1 averaged over all mocks.

4 RESULTS

4.1 Relative velocity constraint

As described in S17b, we compute the 3PCF of the CMASS galaxies and the covariance matrix in the Gaussian random field approximation. We then fit to the 3PCF model based on the bias model in Section 3. We marginalize over α, the value of the BAO scale normalized to a fiducial sound horizon (it is unity if we input the correct cosmology), and over c, a free parameter describing deviations from the integral constraint and also intended to remove any survey-scale systematic bias. The details of our fitting are further described in S17b.

Our fitted parameters are displayed in Tables 1 (data) and 2 (mocks). We constrain the relative velocity bias as $b_v = -0.002 \pm 0.01$. These error bars are computed as the square root of the appropriate diagonal element of the bias covariance matrix as described in S17b.

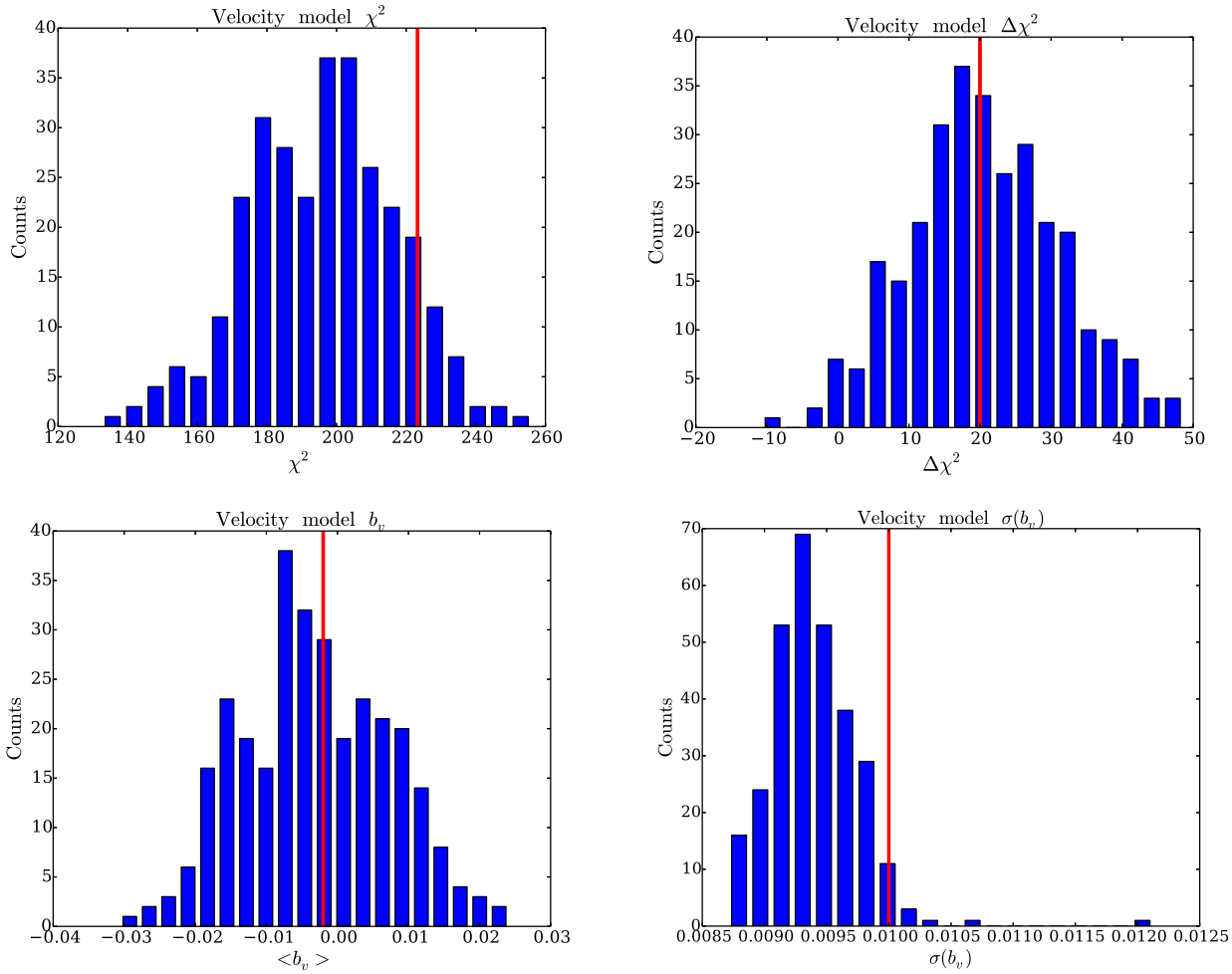

Figure 1. The upper two panels show histograms of the best-fitting χ^2 and the $\Delta\chi^2$ with respect to the best-fitting no-wiggle templates (here, we set $b_v \equiv 0$ for the no-wiggle template) for the 298 PATCHY mocks (S17b, and references therein). The red vertical line indicates the data values. These show that our goodness of fit and BAO significance are both fairly typical for a survey of this volume. The bottom panels histogram the mock results for the relative velocity bias and the root mean square of this bias marginalized over the integral constraint amplitude. The true b_v of all mocks is identically zero, so the 0.01 scatter about zero in the left-hand panel represents one estimate of our error bar on b_v. The estimate of the error as the root mean square of the mocks' b_v, shown in the lower right-hand panel, again indicates 0.01 precision on b_v.

This result is highly consistent with results from two other methods of estimating the error bar. First, we know that the mock catalogues have $b_v \equiv 0$; no relative velocity biasing has been incorporated in them. Our 3PCF fitting returns a mean value of $b_v = 0$, where the mean is taken over the mocks, with a standard deviation of about 0.01, as shown in Fig. 1. Secondly, we can compute $\sigma(b_v)$, the root mean square of the relative velocity bias marginalized over the integral constraint amplitude c for each mock, as described for the other bias parameters in S17b. We then find its average over all mocks as $\langle\sigma(b_v)\rangle = 0.97$. Thus, all three error estimation methods concur that we can constrain the relative velocity bias with 0.01 precision.

We note that the mean b_v from the mocks is $\langle b_v\rangle = -0.0031$, but that this is statistically distinguished from zero at roughly 5σ given the $\sigma \simeq 0.01/\sqrt{298} \approx 0.0006$ error on the mean of the mocks. This issue is similar to the possible systematic difference of the mean $\langle\alpha\rangle$ over all mocks from unity in S17b. This value of $\langle b_v\rangle$ for the mocks indicates that there is a small discrepancy between the bias model and the mocks, which is causing a systematic bias in this b_v term. We will further explore this point with better 3PCF models and more extensive mock catalogues in future work.

4.2 Other bias parameters

We now briefly discuss the other bias parameter values found for the mocks and for the data. As Tables 1 and 2 show, the bias values and error bars we find are generally consistent between mocks and data. There is some disagreement between the error bar for b_1 from the data and from the scatter of the mocks. We achieve a strong constraint on b_1, making a 1.10 per cent precision measurement. We do not obtain a strong constraint on b_2; as discussed in SE17 and S17b, it is highly degenerate with b_1 and so will not be well-measured. The integral constraint amplitude value for the data is consistent with that we find for our minimal model (with $b_v \equiv 0$) in S17b, and this is also the case for the integral constraint amplitude for the mocks.

Regarding the χ^2, for the data we find $\chi^2/\text{d.o.f} = 223.26/195$, indicating that our model fits the data fairly well. For the mocks, we find an average $\chi^2/\text{d.o.f} = 195.34/195$, indicating that the mocks also are well-fit by the model. If the model truly describes the data or mocks, these χ^2 have probabilities P to occur by chance of, respectively, $P = 0.08$ and $P = 0.49$.

Fig. 1 shows the typicality of our results from the data with respect to the mocks. In each panel, the red line indicates the data

Table 1. Table of best-fitting parameters for the CMASS data. b_1, b_2 and b_v are the linear, non-linear and relative velocity biases, and c encodes the integral constraint. $\Delta\chi^2$ describes the χ^2 penalty a no-BAO model pays over a model with BAO. The value listed here implies a 4.49σ BAO detection for the velocity model. α describes the inferred cosmic distance scale. The error bars quoted here are from the square root of the diagonal of the bias covariance matrix $\boldsymbol{C}_{\rm bias}$. Our error bar on the linear bias corresponds to 1.10 per cent.

	Data: velocity
$\Delta\chi^2$	19.99
α	0.990 ± 0.020
b_1	1.776 ± 0.020
b_2	0.52 ± 0.17
b_v	-0.002 ± 0.010
c	-0.014 ± 0.003
χ^2	223.26

Table 2. Table of best-fitting parameters for the mocks. We report the mean of each parameter over the 298 mocks. The error bars on these parameters are the standard deviation of the parameter taken over all mocks; for $\langle\alpha\rangle$, we also report the average of the root mean square $\sigma(\alpha)$ over all mocks in parentheses. For the error bars on the biases, we have held α fixed at its average value over all the mocks, as allowing α to float can artificially inflate the scatter in the biases. This point is further discussed in S17b's section 9. Comparing the error bars here, from the scatter of the 298 mocks, to those reported in Table 1, mostly confirms that the error bars estimated from the bias covariance matrix are reasonable. We further discuss this point in Section 4.

	Mocks: velocity
$\Delta\chi^2$	20.59
α	$1.01 \pm 0.026\,(0.021)$
b_1	1.936 ± 0.030
b_2	0.50 ± 0.21
b_v	-0.0031 ± 0.0097
c	0.000 ± 0.009
χ^2	195.34

value. The upper left-hand panel shows that the χ^2 for our best-fitting model to the data is fairly typical for a survey of this size. The upper right-hand panel shows the difference in χ^2 between the best-fitting no-wiggle template (with $b_v \equiv 0$) and the best-fitting physical template (with BAO, and with b_v free). Our BAO detection in this data set is in the range we would expect for a survey of this size.

The lower left-hand panel of Fig. 1 shows the b_v values measured for the mocks. In truth, the mocks have $b_v = 0$, so any $b_v \neq 0$ we measure indicates the error bar on the b_v constraint derived from the data. As expected, the centre of the mocks' b_v distribution is near $b_v = 0$, and the scatter is 0.01. As Table 1 indicates, for the data we find b_v consistent with zero within our error bars. The lower right-hand panel in Fig. 1 shows the root mean square $\sigma(b_v)$ computed from marginalizing b_v and b_v^2 over the integral constraint amplitude, following the same procedure as outlined for the linear bias in section 5.2 of S17b. The mean $\sigma(b_v)$ is about 0.0097, and the data have $\sigma(b_v) = 0.010$; these values both indicate that we can constrain the relative velocity bias as $b_v < 0.01$.

4.3 Cosmic distance scale

To convert α into a physical distance scale $D_{\rm V}$ to redshift 0.57, we generalize the formula for $D_{\rm V}$ of Anderson et al. (2014) to varying $\Omega_{\rm m}$ and redshift; we also convert to the PATCHY cosmology (S17b and references therein) and from Mpc h^{-1} to Mpc. We find

$$D_{\rm V} = \alpha \times 2054.4\,{\rm Mpc}\left(\frac{r_{\rm d}}{r_{\rm d,\,PATCHY}}\right), \tag{2}$$

where $r_{\rm d}$ is the sound horizon at decoupling and $r_{\rm d,\,PATCHY}$ is the sound horizon at decoupling for the PATCHY cosmology. We thus find

$$D_{\rm V,\,velocity}(z_{\rm survey}) = 2034 \pm 41\,{\rm Mpc\,(stat)} \pm 20\,{\rm Mpc\,(sys)} \times \left(\frac{r_{\rm d}}{r_{\rm d,\,PATCHY}}\right). \tag{3}$$

From fitting the 2PCF of SDSS DR11 including reconstruction, Anderson et al. (2014) found

$$D_{\rm V,\,Anderson}(z_{\rm survey}) = 2034 \pm 20\,{\rm Mpc}\left(\frac{r_{\rm d}}{r_{\rm d,\,PATCHY}}\right), \tag{4}$$

whereas from the SDSS DR12 CMASS 2PCF including reconstruction, Cuesta et al. (2016) found

$$D_{\rm V,\,Cuesta}(z_{\rm survey}) = 2036 \pm 21\,{\rm Mpc}\left(\frac{r_{\rm d}}{r_{\rm d,\,PATCHY}}\right). \tag{5}$$

From the reconstructed multipoles of the CMASS DR12 power spectrum, Gil-Marín et al. (2016) found

$$D_{\rm V,\,Gil-Marin}(z_{\rm survey}) = 2023 \pm 18\,{\rm Mpc}\left(\frac{r_{\rm d}}{r_{\rm d,\,PATCHY}}\right). \tag{6}$$

We have adjusted the measured $D_{\rm V}$'s of these works appropriately to be quoted in terms of our fiducial PATCHY sound horizon.

Our velocity model measurements are therefore highly consistent with the latest 2PCF and power spectrum BAO analysis results. None of the other works we quote incorporated a relative velocity bias in their fitting, but given that our data prefers a b_v that is nearly zero, we indeed expect our velocity model distance scale measurement to be consistent with theirs. Our slightly larger error bars reflect that we achieve a precision of roughly 2.0 per cent on the distance scale, whereas the 2PCF or power spectrum measurements achieve a precision of roughly 1.0 per cent. Our results are also consistent with the measured distance scale in the final cosmological analysis of the SDSS DR12 combined sample (Alam et al. 2017).

5 CONCLUSIONS

We have shown that the 3PCF permits a 0.01 precision measurement of the relative velocity bias, translating to about 0.5 per cent of the linear bias. We have shown three different estimates of this error bar that are all consistent with each other. For the data, we find b_v consistent with zero within our error bars.

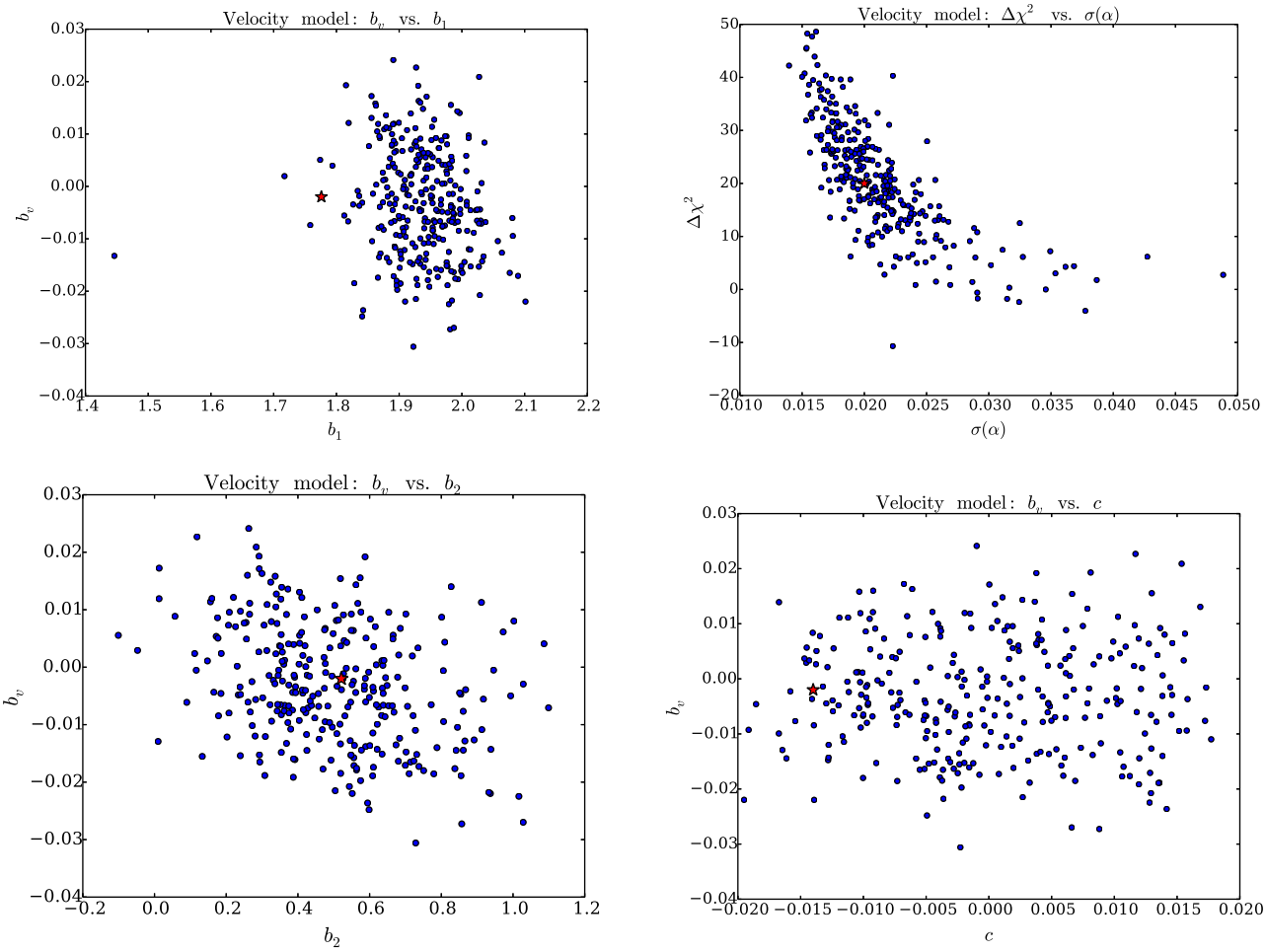

Figure 2. Here, we show several scatter plots illustrating the degeneracy structure of b_v with respect to the other parameters of our fits. In all panels, the data values are marked by a red star. The upper left-hand panel shows that b_v is not highly degenerate with b_1. The lower left-hand panel shows there is an extremely mild anticorrelation between b_2 and b_v. The lower right-hand panel shows that there is no correlation between the integral constraint amplitude c and b_v. The upper right-hand panel shows that as the significance of our BAO detection rises, the root mean square error on α improves, as expected.

The constraint of Yoo & Seljak (2013) from the power spectrum used 260 000 SDSS DR11 galaxies to place the constraint $b_{v,\,\mathrm{YS}} < 0.033$. In their bias model, the relative velocity's square is normalized by its 1D variance, $\sigma^2_{\mathrm{bc,\,1D}}$, which is one-third the 3-D variance σ^2_{bc} used in our bias model (1). Holding the combination $b_v(v^2_{\mathrm{bc}}/\sigma^2_{\mathrm{bc}})$ constant, as this is what enters the bias models, the normalization difference means that their measured b_v should be multiplied by a factor of 3 to be compared with ours. Thus, as we define b_v the Yoo & Seljak (2013) constraint is $b_v < 0.1$. The constraint $b_v < 0.01$ of this work is a factor of 10 tighter.

Were our 3PCF technique equally good as the power spectrum analysis described above, we would expect a 0.58 precision constraint (the precisions simply scale as $\sqrt{N_{\mathrm{g}}}$, with N_{g} the number of galaxies). Finding a 0.01 constraint thus shows the superiority of the 3PCF for these measurements relative to the signature in the power spectrum model used by the Yoo & Seljak analysis by roughly a factor of 6. However, we note that while this work was in the final stages of being refereed, an updated power spectrum constraint (Beutler et al. 2017) appeared, which finds no evidence for a non-zero relative velocity bias and achieved a comparable precision to this work. That work's constraint from the power spectrum is driven primarily by the BMH16-type advection term, which is not present in the tree-level 3PCF used in our analysis or in the Yoo & Seljak (2013) power spectrum constraint discussed above. Consequently, it is reasonable to hope that the power spectrum and 3PCF constraints on the relative velocity bias are independent and can be combined to further tighten the precision, though detailed work with simulations would be desirable to further buttress this intuition.

The relative velocity effect can bias the BAO scale measured in the 2PCF, and thus a tight constraint on b_v is essential for present surveys such as BOSS and future efforts like DESI to remain unbiased. The constraint we find in this work is tight enough that the shift in α measured from the 2PCF will be less than 0.3 per cent, using a recalculation of BMH16 (Fig. 2) for the appropriate linear bias and survey redshift for CMASS to translate b_v/b_1 into a shift in α. The BOSS survey can thus control b_v to a level equivalent to $\sim$1/3 of its BAO statistical precision. For surveys of larger volume at similar number density, this indicates that the RV effect can be sufficiently controlled. We note that care should be exercised in extending this conclusion to a different galaxy population from the one considered here. For instance, naively one might expect that less massive galaxies, such as the Hα or Lyα emitters targeted by ongoing or future experiments such as HETDEX, *Euclid* and PFS, could have a larger relative velocity bias. Performing a 3PCF analysis on those samples would be important as a means of

protecting any BAO-scale measurements against a possibly larger value of the relative velocity bias.

In closing, we highlight that the consistency with zero of our measured b_v for the CMASS data has interesting possible implications for galaxy formation models. Our constraint on b_v suggests that galaxies do not have strong memories of their less-massive high redshift progenitors. Given that only a small fraction of the stars in LRGs at $z \sim 0$ were produced in the high-redshift small haloes most affected by the relative velocity, this finding is not unexpected. Our constraint suggests that feedback is likely efficient at erasing any differences between galaxies formed in high relative velocity regions and low relative velocity regions. Although mergers also play a role in the evolution of small high-redshift haloes into the LRGs used for the BAO, the relative velocity's coherence scale is sufficiently large that we do not expect mergers could by themselves erase a relative velocity imprint. Further exploration of this point may be a worthwhile avenue of future work.

ACKNOWLEDGEMENTS

We thank the referee, Fabian Schmidt, for very useful comments. We also thank Blakesley Burkhart, Cora Dvorkin, Douglas Finkbeiner, Margaret Geller, Abraham Loeb, Philip Mocz, Ramesh Narayan, Stephen Portillo, Roman Scoccimarro, Uroš Seljak, Joshua Suresh, Licia Verde and Martin White for useful conservations. This material is based upon work supported by the National Science Foundation Graduate Research Fellowship under Grant No. DGE-1144152; DJE is supported by grant DE-SC0013718 from the U.S. Department of Energy. JAB is supported by a Center for Cosmology and AstroParticle Physics Fellowship. HG-M acknowledges Labex ILP (reference ANR-10-LABX-63) part of the Idex SUPER, and received financial state aid managed by the Agence Nationale de la Recherche, as part of the programme Investissements d'avenir under the reference ANR-11-IDEX-0004-02. SH is supported by NSF AST1412966, NASA -EUCLID11-0004 and NSF AST1517593 for this work. WJP acknowledges support from the UK Science and Technology Facilities Research Council through grants ST/M001709/1 and ST/N000668/1, the European Research Council through grant 614030 Darksurvey and the UK Space Agency through grant ST/N00180X/1. GR acknowledges support from the National Research Foundation of Korea (NRF) through NRF-SGER 2014055950 funded by the Korean Ministry of Education, Science and Technology (MoEST) and from the faculty research fund of Sejong University in 2016. F-SK acknowledges support from the Leibniz Society for the Karl-Schwarzschild fellowship.

Funding for SDSS-III has been provided by the Alfred P. Sloan Foundation, the Participating Institutions, the National Science Foundation and the U.S. Department of Energy Office of Science. The SDSS-III web site is http://www.sdss3.org/.

SDSS-III is managed by the Astrophysical Research Consortium for the Participating Institutions of the SDSS-III Collaboration including the University of Arizona, the Brazilian Participation Group, Brookhaven National Laboratory, Carnegie Mellon University, University of Florida, the French Participation Group, the German Participation Group, Harvard University, the Instituto de Astrofisica de Canarias, the Michigan State/Notre Dame/JINA Participation Group, Johns Hopkins University, Lawrence Berkeley National Laboratory, Max Planck Institute for Astrophysics, Max Planck Institute for Extraterrestrial Physics, New Mexico State University, New York University, Ohio State University, Pennsylvania State University, University of Portsmouth, Princeton University, the Spanish Participation Group, University of Tokyo, University of Utah, Vanderbilt University, University of Virginia, University of Washington and Yale University.

REFERENCES

Abazajian K. N. et al., 2009, ApJS, 182, 543
Aihara H. et al., 2011, ApJS, 193, 29
Alam S. et al., 2015, ApJS, 219, 12
Alam S. et al., 2017, MNRAS, 470, 2617
Anderson L. et al., 2014, MNRAS, 441, 24
Beutler F., Blake C., Koda J., Marín F., Seo H.-J., Cuesta A. J., Schneider D., 2016, MNRAS, 455, 3230
Beutler F., Seljak U., Vlah Z., 2017, MNRAS, 470, 2723
Blanton M., Lin H., Lupton R. H., Maley F. M., Young N., Zehavi I., Loveday J., 2003, AJ, 125, 2276
Blazek J., McEwen J., Hirata C., 2016, PRL, 116, 12, 121303 (BMH16)
Bolton A. et al., 2012, AJ, 144, 144
Bond J. R., Efstathiou G., 1984, ApJ, 285, L45
Bond J. R., Efstathiou G., 1987, MNRAS, 226, 655
Cuesta A. J. et al., 2016, MNRAS, 457, 1770
Dalal N., Pen U., Li U.-L., 2010, JCAP, 11, 007
Dawson K. et al., 2013, AJ, 145, 10
Doi M. et al., 2010, AJ, 139, 1628
Eisenstein D. J., Hu W., 1998, ApJ, 496, 605
Eisenstein D. J., Seo H.-J., White M., 2007, ApJ, 664, 660
Eisenstein D. J. et al., 2011, AJ, 142, 72
Fukugita M. et al., 1996, AJ, 111, 1748
Gil-Marín H. et al., 2016, MNRAS, available at: doi:10.1093/mnras/stw1264
Gunn J. E. et al., 1998, AJ, 116, 3040
Gunn J. E. et al., 2006, AJ, 131, 2332
Holtzmann J. A., 1989, ApJS, 71, 1
Hu W., Sugiyama N., 1996, ApJ, 471, 542
Kitaura F.-S., Heß S., 2013, MNRAS, 435, L78
Kitaura F.-S., Yepes G., Prada F., 2014, MNRAS, 439, L21
Kitaura F.-S., Gil-Marín H., Scóccola C. G., Chuang C.-H., Müller V., Yepes G., Prada F., 2015, MNRAS, 450, 1836
Kitaura F.-S. et al., 2016, MNRAS, 456, 4156
Levi M. et al., 2013, preprint (arXiv:1308.0847)
Lewis A., 2000, ApJ, 538, 473
Lupton R., Gunn J. E., Ivezic Z., Knapp G., Kent S., 2001, in Harnden F. R., Jr, Primini F. A., Payne H. E., eds, ASP Conf. Proc. Vol. 238, The SDSS Imaging Pipelines. Astron. Soc. Pac., San Francisco, p. 269
Padmanabhan N. et al., 2008, ApJ, 674, 1217
Peebles P. J. E., Yu J. T., 1970, ApJ, 162, 815
Pier J. R. et al., 2003, AJ, 125, 1559
Reid B. et al., 2016, MNRAS, 455, 1553
Rodríguez-Torres S. et al., 2016, MNRAS, 460, 1173
Ross A. J. et al., 2017, MNRAS, 464, 1168
Sakharov A. D., 1966, Sov. J. Exp. Theor. Phys., 22, 241
Schmidt F., 2016, PRD, 94, 063508 (S16)
Slepian Z., Eisenstein D. J., 2015a, MNRAS, 448, 9 (SE15a)
Slepian Z., Eisenstein D. J., 2015b, MNRAS, 454, 4142
Slepian Z., Eisenstein D. J., 2015c, MNRAS, 455, L31
Slepian Z., Eisenstein D. J., 2016, MNRAS, 457, 24
Slepian Z., Eisenstein D. J., 2017, MNRAS, 469, 2059 (SE17)
Slepian Z. et al., 2017a, MNRAS, 468, 1070
Slepian Z. et al., 2017b, MNRAS, 469, 1738 (S17b)
Smee S. A. et al., 2013, AJ, 126, 32
Smith J. A. et al., 2002, AJ, 123, 2121
Sunyaev R. A., Zel'dovich Ya. B., 1970, Ap&SS, 7, 3
Tseliakhovich D., Hirata C., 2010, Phys. Rev. D, 82, 083520
Yoo J., Seljak U., 2013, Phys. Rev. D, 88, 10, 103520
Yoo J., Dalal N., Seljak U., 2011, J. Cosmol. Astropart. Phys., 7, 018
York D. G. et al., 2000, AJ, 120, 1579

This paper has been typeset from a TEX/LATEX file prepared by the author.